Reconstruction of an astigmatic hard X-ray beam and alignment of K-B mirrors from ptychographic coherent diffraction data

Cameron M. Kewish,[1,5,*] Manuel Guizar-Sicairos,[2,6] Chian Liu,[3] Jun Qian,[3] Bing Shi,[3] Christa Benson,[4] Ali M. Khounsary,[4] Joan Vila-Comamala,[1] Oliver Bunk,[1] James R. Fienup,[2] Albert T. Macrander,[3] and Lahsen Assoufid[3]

[1]Paul Scherrer Institut, CH-5232 Villigen PSI, Switzerland
[2]The Institute of Optics, University of Rochester, Rochester, New York 14627, USA
[3]X-ray Science Division, Argonne National Laboratory, Argonne, Illinois 60439, USA
[4]APS Engineering Support Division, Argonne National Laboratory, Argonne, Illinois 60439, USA
[5]Current address: Synchrotron SOLEIL, Saint Aubin BP-48, F-91192 Gif-sur-Yvette, France
[6]Current address: Paul Scherrer Institut, CH-5232 Villigen PSI, Switzerland
[*]Cameron.Kewish@synchrotron-soleil.fr

Abstract: We have used coherent X-ray diffraction experiments to characterize both the 1-D and 2-D foci produced by nanofocusing Kirkpatrick-Baez (K-B) mirrors, and we find agreement. Algorithms related to ptychography were used to obtain a 3-D reconstruction of a focused hard X-ray beam waist, using data measured when the mirrors were not optimally aligned. Considerable astigmatism was evident in the reconstructed complex wavefield. Comparing the reconstructed wavefield for a single mirror with a geometrical projection of the wavefront errors expected from optical metrology data allowed us to diagnose a 40 μrad misalignment in the incident angle of the first mirror, which had occurred during the experiment. Good agreement between the reconstructed wavefront obtained from the X-ray data and off-line metrology data obtained with visible light demonstrates the usefulness of the technique as a metrology and alignment tool for nanofocusing X-ray optics.

OCIS codes: (100.5070) Phase retrieval; (340.0340) X-ray optics; (140.3295) Laser beam characterization; (340.7470) X-ray mirrors; (110.3200) Inverse scattering.

References and links

1. H. M. Quiney, A. G. Peele, Z. Cai, D. Paterson, and K. A. Nugent, "Diffractive imaging of highly focused X-ray fields," Nat. Phys. **2**(2), 101–104 (2006).
2. H. Yumoto, H. Mimura, S. Matsuyama, S. Handa, Y. Sano, M. Yabashi, Y. Nishino, K. Tamasaku, T. Ishikawa, and K. Yamauchi, "At-wavelength figure metrology of hard X-ray focusing mirrors," Rev. Sci. Instrum. **77**(6), 063712 (2006).
3. P. Thibault, M. Dierolf, A. Menzel, O. Bunk, C. David, and F. Pfeiffer, "High-resolution scanning X-ray diffraction microscopy," Science **321**(5887), 379–382 (2008).
4. M. Guizar-Sicairos, and J. R. Fienup, "Phase retrieval with transverse translation diversity: a nonlinear optimization approach," Opt. Express **16**(10), 7264–7278 (2008).
5. P. Thibault, M. Dierolf, O. Bunk, A. Menzel, and F. Pfeiffer, "Probe retrieval in ptychographic coherent diffractive imaging," Ultramicroscopy **109**(4), 338–343 (2009).
6. A. M. Maiden, and J. M. Rodenburg, "An improved ptychographical phase retrieval algorithm for diffractive imaging," Ultramicroscopy **109**(10), 1256–1262 (2009).
7. M. Guizar-Sicairos, and J. R. Fienup, "Measurement of coherent X-ray focused beams by phase retrieval with transverse translation diversity," Opt. Express **17**(4), 2670–2685 (2009).
8. C. M. Kewish, P. Thibault, M. Dierolf, O. Bunk, A. Menzel, J. Vila-Comamala, K. Jefimovs, and F. Pfeiffer, "Ptychographic characterization of the wavefield in the focus of reflective hard X-ray optics," Ultramicroscopy **110**(4), 325–329 (2010).
9. A. Schropp, P. Boye, J. M. Feldkamp, R. Hoppe, J. Patommel, D. Samberg, S. Stephan, K. Giewekemeyer, R. N. Wilke, T. Salditt, J. Gulden, A. P. Mancuso, I. A. Vartanyants, E. Weckert, S. Schöder, M. Burghammer, and C. G. Schroer, "Hard X-ray nanobeam characterization by coherent diffraction microscopy," Appl. Phys. Lett. **96**(9), 091102 (2010).

10. M. Guizar-Sicairos, K. Evans-Lutterodt, A. F. Isakovic, A. Stein, J. B. Warren, A. R. Sandy, S. Narayanan, and J. R. Fienup, "One-dimensional hard X-ray field retrieval using a moveable structure," Opt. Express **18**(17), 18374–18382 (2010).
11. A. Souvorov, M. Yabashi, K. Tamasaku, T. Ishikawa, Y. Mori, K. Yamauchi, K. Yamamura, and A. Saito, "Deterministic retrieval of surface waviness by means of topography with coherent X-rays," J. Synchrotron Radiat. **9**(Pt 4), 223–228 (2002).
12. K. Yamauchi, K. Yamamura, H. Mimura, Y. Sano, A. Saito, K. Endo, A. Souvorov, M. Yabashi, K. Tamasaku, T. Ishikawa, and Y. Mori, "Wave-optical evaluation of interference fringes and wavefront phase in a hard-X-ray beam totally reflected by mirror optics," Appl. Opt. **44**(32), 6927–6932 (2005).
13. C. M. Kewish, L. Assoufid, A. T. Macrander, and J. Qian, "Wave-optical simulation of hard-X-ray nanofocusing by precisely figured elliptical mirrors," Appl. Opt. **46**(11), 2010–2021 (2007).
14. C. M. Kewish, A. T. Macrander, L. Assoufid, and J. Qian, "Comparison of two methods for simulation of hard X-ray nanofocusing by elliptical mirrors," Nucl. Instrum. Methods Phys. Res. A **582**(1), 138–141 (2007).
15. H. Mimura, H. Yumoto, S. Matsuyama, S. Handa, T. Kimura, Y. Sano, M. Yabashi, Y. Nishino, K. Tamasaku, T. Ishikawa, and K. Yamauchi, "Direct determination of the wave field of an X-ray nanobeam," Phys. Rev. A **77**(1), 015812 (2008).
16. W. Chao, B. D. Harteneck, J. A. Liddle, E. H. Anderson, and D. T. Attwood, "Soft X-ray microscopy at a spatial resolution better than 15 nm," Nature **435**(7046), 1210–1213 (2005).
17. C. G. Schroer, O. Kurapova, J. Patommel, P. Boye, J. Feldkamp, B. Lengeler, M. Burghammer, C. Riekel, L. Vincze, A. van der Hart, and M. Küchler, "Hard X-ray nanoprobe based on refractive X-ray lenses," Appl. Phys. Lett. **87**(12), 124103 (2005).
18. H.-C. Kang, J. Maser, G. B. Stephenson, C. Liu, R. Conley, A. T. Macrander, and S. Vogt, "Nanometer linear focusing of hard x rays by a multilayer Laue lens," Phys. Rev. Lett. **96**(12), 127401 (2006).
19. H. Mimura, H. Yumoto, S. Matsuyama, Y. Sano, K. Yamamura, Y. Mori, M. Yabashi, Y. Nishino, K. Tamasaku, T. Ishikawa, and K. Yamauchi, "Efficient focusing of hard X-rays to 25 nm by a total reflection mirror," Appl. Phys. Lett. **90**(5), 051903 (2007).
20. I. K. Robinson, F. Pfeiffer, I. A. Vartanyants, Y. Sun, and Y. Xia, "Enhancement of coherent X-ray diffraction from nanocrystals by introduction of X-ray optics," Opt. Express **11**(19), 2329–2334 (2003).
21. Y. Takahashi, Y. Nishino, H. Mimura, R. Tsutsumi, H. Kubo, T. Ishikawa, and K. Yamauchi, "Feasibility study of high-resolution coherent diffraction microscopy using synchrotron X-rays focused by Kirkpatrick-Baez mirrors," J. Appl. Phys. **105**(8), 083106 (2009).
22. K. Yamauchi, H. Mimura, K. Inagaki, and Y. Mori, "Figuring with subnanometer-level accuracy by numerically controlled elastic emission machining," Rev. Sci. Instrum. **73**(11), 4028–4033 (2002).
23. C. Liu, L. Assoufid, R. Conley, A. T. Macrander, G. E. Ice, and J. Z. Tischler, "Profile coating and its application for Kirkpatrick-Baez mirrors," Opt. Eng. **42**(12), 3622–3628 (2003).
24. G. R. Brady, M. Guizar-Sicairos, and J. R. Fienup, "Optical wavefront measurement using phase retrieval with transverse translation diversity," Opt. Express **17**(2), 624–639 (2009).
25. F. Pfeiffer, O. Bunk, C. Schulze-Briese, A. Diaz, T. Weitkamp, C. David, J. F. van der Veen, I. Vartanyants, and I. K. Robinson, "Shearing interferometer for quantifying the coherence of hard X-ray beams," Phys. Rev. Lett. **94**(16), 164801 (2005).
26. S. Gorelick, V. A. Guzenko, J. Vila-Comamala, and C. David, "Direct e-beam writing of dense and high aspect ratio nanostructures in thick layers of PMMA for electroplating," Nanotechnology **21**(29), 295303 (2010).
27. Manufactured by Dectris Ltd.: Neuenhoferstrasse 107, CH-5400 Baden, Switzerland. *Model: PILATUS 2M*.
28. Ch. Broennimann, E. F. Eikenberry, B. Henrich, R. Horisberger, G. Huelsen, E. Pohl, B. Schmitt, C. Schulze-Briese, M. Suzuki, T. Tomizaki, H. Toyokawa, and A. Wagner, "The PILATUS 1M detector," J. Synchrotron Radiat. **13**(Pt 2), 120–130 (2006).
29. P. Kraft, A. Bergamaschi, Ch. Broennimann, R. Dinapoli, E. F. Eikenberry, B. Henrich, I. Johnson, A. Mozzanica, C. M. Schlepütz, P. R. Willmott, and B. Schmitt, "Performance of single-photon-counting PILATUS detector modules," J. Synchrotron Radiat. **16**(Pt 3), 368–375 (2009).
30. V. Elser, "Phase retrieval by iterated projections," J. Opt. Soc. Am. A **20**(1), 40–55 (2003).
31. V. Elser, I. Rankenburg, and P. Thibault, "Searching with iterated maps," Proc. Natl. Acad. Sci. U.S.A. **104**(2), 418–423 (2007).

1. Introduction

The ability to characterize a coherent focused X-ray beam [1−10] has important applications in X-ray imaging and optics fabrication. Because the aberrations in the wavefronts can be related to the optical quality of a focusing element [11−15], this provides useful feedback on how certain fabrication tolerances affect the focusing performance at the wavelength of interest. The push for smaller focal spots in the hard X-ray regime is closely linked to improvements in fabrication technology (see, *e.g.*, [16−19]), and when multiple focusing devices are used to achieve a two-dimensional (2-D) focus, the alignment between the elements is perhaps of even more critical importance. It is therefore important to have a reliable method for beam characterization that can be implemented *in situ* to directly assess the quality of the focused beam.

The use of Kirkpatrick-Baez (K-B) mirrors as focusing elements for coherent diffraction experiments was first reported in experiments using Bragg reflection in a synchrotron facility [20]. More recently, it was proposed that the high reflection efficiency of K-B mirrors could be exploited in diffraction microscopy, to create a beam with sufficient photon density at the sample to allow sub-1 nm resolution to be achieved [21]. In practice this would require very high quality mirrors, aligned to within microradians of their designed incidence angles. Technically, the fabrication of such mirrors is within reach of existing X-ray optics fabrication techniques which can produce nanofocusing K-B mirrors with < 1 nm-rms deviations from ideally elliptical [22,23]. However, the alignment of X-ray optics is often done effectively by trial-and-error, guided by knife-edge scans of the focus or images of test objects.

Coherent diffractive imaging methods are unique in their ability to recover the complex wavefield distribution in the beam from one or more far-field intensity measurements. Numerically propagating the reconstructed wavefield additionally reveals information about misalignments or larger scale aberrations in the whole optical system. Here we describe methods we have used to characterize both 1-D and 2-D foci produced by state-of-the-art K-B mirrors, reconstruct the surface aberrations in a single mirror with between 0.58 nm-rms and 1.56 nm-rms surface imperfections, and diagnose a grazing angle misalignment of 40 μrad.

Two methods were used. First, a 3-D beam reconstruction was obtained using ptychography, a method we have used in the past to reconstruct a HeNe laser beam and sub-micrometer-sized X-ray foci (see [5,8,24] for details). A similar approach employing a different algorithm has also been demonstrated [6,9]. The novel aspect of our result is that it demonstrates the success of ptychographic beam characterization under conditions of aberration, astigmatism and misalignment. Second, a 2-D nanobeam reconstruction was obtained for a single mirror using a one-dimensional version of a nonlinear optimization algorithm referred to as phase-retrieval with transverse translation diversity [4,10]. From our results it was possible to quantify aberrations in the focused wavefield which resulted from fabrication and positioning errors. This permitted us to calculate by how much a single mirror should be realigned in order to achieve a better focus, despite having almost-diffraction limited performance as judged from the focal spot intensity profile. Further, we could calculate for a pair of mirrors the adjustment required to remove astigmatism. These are questions that can be conveniently answered by reconstructing the focused wavefield. The results furthermore suggest an efficient and accurate method of optimizing the alignment of nanofocusing X-ray optics. This places ptychography into a new context as a tool which can be used for beamline alignment and optical diagnostics in addition to X-ray imaging and beam characterization.

2. Mirror design and experimental setup

Two elliptical mirrors were fabricated by profile-coating, *i.e.*, selectively depositing an elliptical surface of Pt onto Si substrates [23]. The first mirror, M1, vertically focuses the X-ray beam while the second, M2, focuses horizontally. We can completely specify the elliptical profile of the mirrors $h(z_m)$, as a function of position z_m, along the reflecting surface length L, using three parameters; the source-to-mirror distance s_1, the mirror-to-focus distance s_2, and the grazing angle of incidence of the X-rays at the lowest point on the mirror surface, θ_0. Table 1 lists these parameters for the best-fit ellipse to micro-stitched interferometric surface height data for each mirror, and the rms departure from elliptical, Δh. Wave-optical calculations [13,14] were employed to predict the focal spot full-width at half-maximum (fwhm), w, and the depth-of-focus, d, which we define as twice the Rayleigh length. The first two rows of data in Table 1 indicate the parameters for the best-fit ellipse to M1, where the first is a fit over the best 73 mm of the surface, and the second is a fit to the best 56.6 mm of the surface; the differences in w and d illustrate that the surface quality varies with position.

Table 1. Best-fit ellipse parameters for the profile coated K-B mirror pair, where Δ*h* represents the rms departure from the best-fit ellipse, *w* is the simulated fwhm of the focus, and *d* is the simulated depth-of-focus.

Mirror	L [mm]	$s_1{}^a$ [m]	s_2 [mm]	θ_0 [mrad]	$\Delta h(z_m)$ [nm]	w [nm]	d [μm]
M1	73.0	34.425	93.12	2.99	1.56	71	180
	56.6	34.425	93.02	2.99	0.58	110	400
M2	10.0	34.500	19.29	3.23	0.80	105	420

^{a} Source distance s_1 was fixed during fitting.

Coherent diffraction experiments were carried out at the cSAXS beamline at the Swiss Light Source. The radiation source is approximately 200(horizontal) × 20(vertical) μm^2 in fwhm at the undulator, which at the selected wavelength λ = 2 Å (Δ*E*/*E* ~10^{-4}), provides coherent radiation over an area of 30(h) × 300(v) μm^2 transverse to the beam in the experiment hutch 34.5 m downstream [25]. A coherent portion of the beam 15(h) × 210(v) μm^2 in area was selected using slits.

A schematic of the experiment geometry is shown in Fig. 1. The K-B mirrors were mounted in the experiment hutch at the distances s_1 from the undulator, as listed in Table 1.
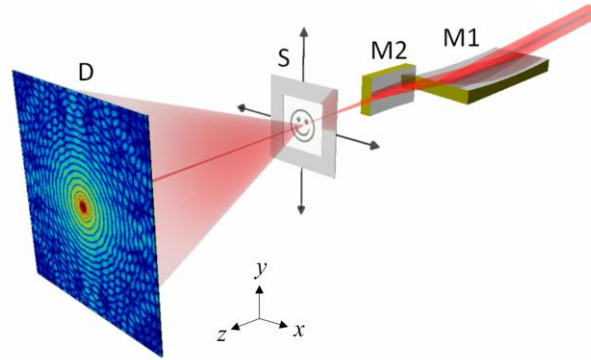
Fig. 1. Schematic diagram of the experiment geometry for characterization of a nanobeam produced by K-B mirrors. The X-ray beam is incident from the right, and is focused by a K-B mirror pair (M1, M2) onto the sample (S). The sample is a nanofabricated Au test pattern, which can be translated in the plane perpendicular to the beam. The diffracted beam is incident on a detector (D), located several meters downstream. The horizontally focusing mirror M2 was removed for some of the measurements.

Mirror M1 was fixed in position, and the mirror assembly was positioned with a hexapod so that the surface of M1 made a grazing angle of 3 mrad to the incident beam. A positioning system, based on flexure hinges driven by pico-motors with laser interferometers for position readout, was used to position mirror M2 relative to M1. Although this provided accurate relative movements, M2 was not mounted kinematically, and no attempt was made to calibrate or correct its absolute alignment. The mirrors were enclosed in a He environment to protect the reflecting surfaces from damage by the synchrotron beam. A sample consisting of free-standing 1.3 μm-thick Au nanostructure test patterns [26] with lateral features in the 0.5-50 μm range was fabricated on a 200 nm-thick silicon-nitride membrane; an example structure is shown below in Fig. 3(b). This sample thickness was designed to provide approximately π radians of phase shift, and 50% amplitude transmission at 2 Å wavelength. The sample was scanned in the vicinity of the focal plane using a piezoelectric positioning stage. A He-filled tube was used to reduce scattering and absorption along the D = 7.31 m path to the noise-free photon-counting area detector [27–29].

3. Two-dimensional focusing

A coherent hard X-ray 2-D nanofocus was prepared using both mirrors. The beam waist at the focal plane of M1 was expected to be close-to optimum at around 70-100 nm, depending on the part of the surface illuminated. The focus of M2 was expected to be several times larger than the nominal value, not only due to misalignment but also because the incident beam was not large enough to entirely fill the mirror surface, reducing the numerical aperture by half. Moreover, the magnification ratio s_2/s_1 indicates that the focal plane of M2 should contain an image of the source rather than a diffraction limited spot.

Coherent diffraction patterns were recorded as the sample was scanned through the focused beam in steps which ensured at least 50% illumination overlap between neighboring scan positions. A ptychographic reconstruction algorithm [3,5] based on the difference-map [30,31] was used to reconstruct the wavefield of the beam incident on the sample. As a starting point, the probe was assumed to be an ideal focal spot in the plane of the sample with widths w corresponding to the simulated values given in Table 1. The probe function was updated at each iteration. The central 512×512 pixels of each diffraction pattern were filled with statistically significant diffracted intensity. For a detector pixel width, $p_{det} = 172$ μm, this detector area defines a reconstructed pixel size, $p_{rec} = \lambda D/(512 p_{det})$, of 16.6 nm.
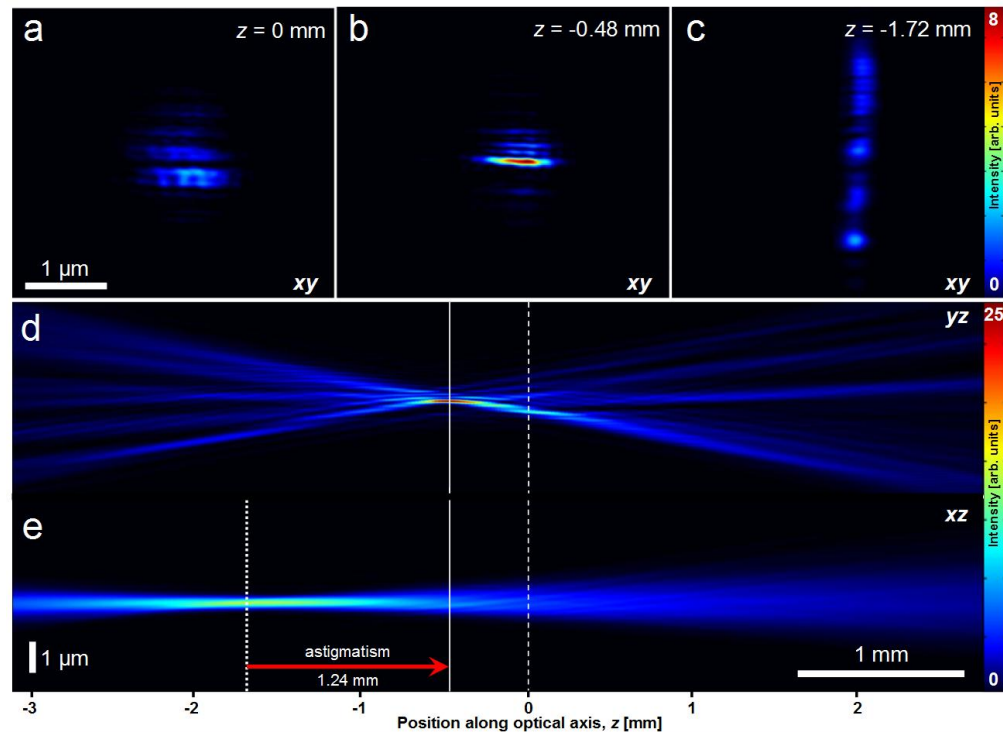
Fig. 2. Reconstruction of an astigmatic hard X-ray nanobeam focused by mirrors M1 and M2. (a) Ptychograph of the wavefield intensity at the sample plane, $(x, y, 0 \text{ mm})$; (b) the vertical focus is 83 nm-fwhm, located at $(x, y, -0.48 \text{ mm})$; (c) the horizontal focus is 232 nm-fwhm, and located at $(x, y, -1.72 \text{ mm})$; (d) beam intensity integrated along the x-direction, showing the vertical beam waist in the yz plane; (e) intensity integrated along the y-direction showing the horizontal beam waist in the xz plane. The red arrow indicates the 1.24 mm separation of the foci. Images (a-c) have the same spatial and intensity scales, as indicated, and the relative position along the optical axis is indicated in the upper right-hand corner of each image. These positions are marked on the orthogonal views (d) and (e) with a dashed line for the sample, a solid line for the vertical focus and a dotted line for the horizontal focus.

Figure 2(a) shows the beam reconstructed at the plane of the sample filling an area of about 680(h) × 230(v) nm², with significant side-lobe structures surrounding the beam. The

astigmatism in this beam comes from a misalignment of mirror M2. Numerically propagating this wavefield along the optical axis by −0.48 mm revealed an intensity maximum at the vertical focus, which was 490(h) × 83(v) nm^2 in size (Fig. 2(b)). Approximately 1.24 mm further upstream of this plane, the horizontal focus was found to be very structured and filling a region 232(h) × 2500(v) nm^2 in size (Fig. 2(c)). The distance between the two foci is the relative translation that would be required to remove the astigmatism. This translation could be achieved by a combination of varying the incidence angle to optimize the focal spot shapes and translating the mirrors relative to each other.

Figure 2(d) shows a view of the beam as projected onto the vertical plane intersecting the optical axis, illustrating the beam waist in the vertical direction and the location of the M1 focus. Figure 2(e) shows the corresponding view from above, indicating the aberrated and elongated horizontal beam waist, and illustrating with a red arrow the 1.24 mm separation of the foci.

4. One-dimensional focusing

To characterize the 1-D focus of a single mirror, the horizontal focusing mirror M2 was removed from the beam. Coherent diffraction patterns, similar to those shown in Fig. 3(a), were measured as a linear sample consisting of a series of horizontal bars (40 × 1 × 1.3) μm^3 in size (Fig. 3(b)) was translated in the vertical direction through the focus in 100 nm steps. The structures were very elongated in the *x*-direction to intercept the whole focus width, in order to provide data for one-dimensional phase retrieval. Some of the far-field intensities were obscured by gaps between the PILATUS detector modules, as shown in Fig. 3(a), so the scan was repeated after the detector had been vertically translated. The combined diffracted intensities were integrated along the non-focusing (*x*) direction, and a one-dimensional nonlinear optimization algorithm was used to reconstruct the focused beam profile [4,10]. The high quality of the PILATUS data alleviated convergence problems observed in earlier 1-D experiments [10] and the solution was consistent under different starting guesses for the beam (e.g. small random numbers and Gaussians of different widths).
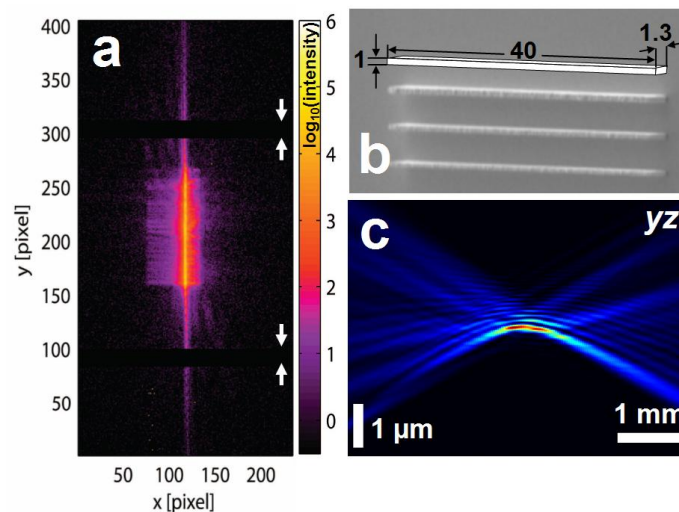
Fig. 3. Reconstruction of a linear focus from mirror M1. (a) Example of the diffraction pattern of the linear test object, in which the gaps between detector modules are indicated with white arrows; (b) scanning electron micrograph of the test object, annotated to show the dimensions of the sample in micrometers; (c) Vertical beam waist obtained by 1-D phase retrieval.

Figure 3(c) shows the intensity in the beam waist, calculated by numerically propagating the reconstructed complex wavefield along the optical axis. The focal spot width in this case was calculated to be 95 nm. This agrees reasonably well with the 83 nm beam size obtained in

the 3-D beam reconstruction shown in Fig. 2(d). The difference could be attributed to small variations in the experiment conditions, because the data sets were measured several hours apart, and during the intervening time the K-B mirror box was opened, closed and re-flushed with He several times.

Simulations (not shown) confirmed that the dominant aberration to the focus seen in Figs. 2(d) and 3(c), *i.e.*, an asymmetry in the focus with large side-lobes on one side of the main peak, results from misalignment in grazing incidence angle. Aberrations of a similar form appear for ideal mirrors misaligned in θ by angles of the order of microradians. This effect is stronger for shorter focal length mirrors, because the apparent figure error between the ideal alignment and the rotated mirror surface increases for more curved surfaces. Backpropagating the reconstructed wavefield to the exit pupil plane, which we define as $z = -s_2$ relative to the focal plane, gives us the amplitude and phase distribution, or wavefront, of the beam leaving the mirror. The amplitude is shown in Fig. 4(a), and the wavefront deviation from spherical is shown in Fig. 4(b). Over the dimensions of the exit pupil of the mirrors, the beam is very well approximated by paraxial optics, and it is possible to relate the figure error measured by interferometry to the phase-retrieval wavefront using a geometrical projection [13]. A mismatch between the wavefronts calculated from phase-retrieval and from the metrology data revealed a pronounced low-order aberration in the phase-retrieval result, which is typical of a misaligned optical system. Optimizing over the grazing incidence angle indicated that the aberrations were consistent with a misalignment of $\Delta\theta = 40$ μrad, which also corresponds to a longitudinal shift of the focus by -1.2 mm. The wavefront computed from the metrology data when we incorporated this misalignment showed good agreement with the backpropagated phase-retrieval result. Very good quantitative agreement is evident in regions where the illumination is high, which can be seen by comparing the Figs. 4(a) and 4(b) in the range $x \in$ $(-50, 180)$ μm. To quantify this comparison, the rms phase difference between the two wavefronts was weighted by the beam intensity to account for the regions where the mirror was not strongly illuminated. The phase difference computed in this fashion is $\sigma_{rms} = 0.27$ rad, or 0.043 waves. We note that for this comparison we have matched a constant, linear, and quadratic phases. At this plane, transverse to the direction of propagation, the beam is very well approximated by paraxial optics and these operations are reasonable.
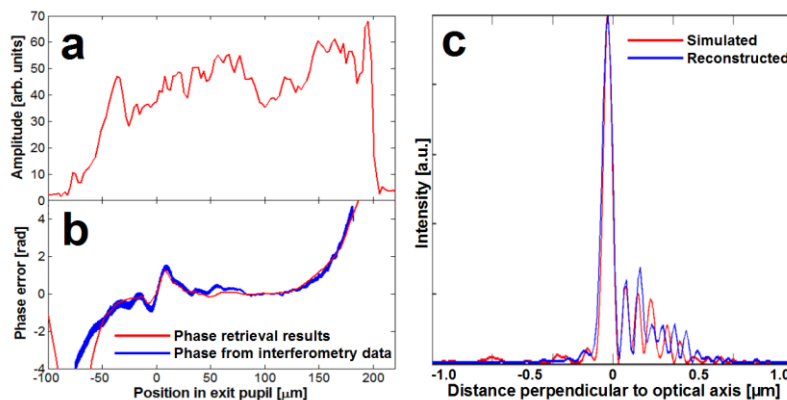
Fig. 4. Comparison of phase-retrieval results with metrology data. (a) Amplitude of the wavefield in the exit pupil plane at $z = -s_2$ relative to the focal plane; (b) the wavefront aberration from phase-retrieval is overlaid with the phase error calculated from visible light metrology data, including a misalignment of 40 μrad; (c) Comparison of the retrieved focus intensity with the simulated intensity: The focal spot widths are 95 nm and 86.4 nm in fwhm, respectively.

The intensity profile in the focal plane, shown in Fig. 4(c) compares quite well with the 86.4 nm-fwhm intensity profile calculated using the metrology data and wave optical calculations assuming a misalignment of 40 μrad in the angle of incidence to a point source

[14]. The difference between these intensity profiles can be attributed to a slight shift of the illumination relative to the section of metrology data used to simulate the mirror surface, evident at the right hand side of Figs. 4(a) and 4(b).

5. Conclusion

In summary, we find that 2-D and 1-D phase retrieval reconstructions were not only able to accurately assess the mirror performance due to the figure errors but they also allowed us to quantitatively deduce the mirror misalignment. This capability will make this technique a very valuable tool for alignment of nanofocusing optics. Moreover, the accuracy with which one can recover the wavefronts in the exit pupil of the optical system, and thereby obtain information about the quality of the focusing optics as a function of position, will provide a useful addition to X-ray wavelength metrology techniques and coherent beam diagnostics, for example at X-ray free electron laser sources.